Cu-doped ZnO as efficient photocatalyst for the oxidation of arsenite to arsenate under visible light

V. Vaiano[a], G. Iervolino[a,*], L. Rizzo[b]

[a] Department of Industrial Engineering, University of Salerno, via Giovanni Paolo II, 132, 84084 Fisciano, SA, Italy
[b] Department of Civil Engineering, University of Salerno, via Giovanni Paolo II, 132, 84084 Fisciano, SA, Italy

ABSTRACT

In this work, photocatalytic oxidation of As(III) to As(V) by ZnO photocatalyts doped with Cu was investigated under visible light. Photocatalysts were successfully prepared by precipitation method. The obtained samples were characterized by N_2 adsorption at -196 C, X-Ray fluorescence analysis, X-ray diffraction, Raman spectroscopy, scanning electron microscopy and UV–vis reflectance analysis. In particular, according to XRD analysis, all samples showed an hexagonal wurtzite structure with average crystallite sizes approximately in the range 32–33 nm. The doping with Cu allowed to obtain a decrease of band gap energy from 3.2 eV, typical of pure ZnO, to 2.92 eV. Photocatalytic oxidation tests under visible light showed that undoped ZnO is not able to oxidize the As(III) present in solution, while the complete conversion of As(III) to As(V) was achieved in the presence of Cu doped ZnO photocatalyst. The best photocatalytic activity was observed with ZnO doped with 1.08 mol% of Cu (1.08Cu_ZnO), within 120 min of exposure to visible light irradiation. The same result was observed under solar simulated radiation. Photocatalytic tests were carried out also in real drinking water and complete oxidation of As(III) to As(V) by 1.08Cu_ZnO photocatalyst was achieved in 120 min under both visible light (emitted by LEDs) and solar simulated radiation.

1. Introduction

Arsenic is a very common element which can be found in rocks, water, air, animals and plants [1]. The toxic and carcinogenic effects of this element are well known, making it a serious threat to the environment and human health [2]. To minimize arsenic related health risks, the World Health Organization (WHO) set the limit of maximum arsenic concentration in drinking water as low as $10 \,\mu g \, L^{-1}$ [3,4]. The prevalent forms of inorganic arsenic naturally occurring in drinking water are As(III) (arsenite), and As(V) (arsenate) [5]. As(III) more toxic, soluble, and mobile than As (V), generally predominates in groundwater [6]. Several processes/technologies have been used for arsenic removal from water so far, such as precipitation, adsorption, ion exchange and membrane systems [7,8]. The main problem related to these processes is that they are effective only on the removal of As(V). So, the use of a pre-oxidation step is necessary to oxidize As(III) to As (V) in order to achieve the total arsenic removal with a subsequent separation process [9]. Oxidation can be achieved by conventional oxidants such as ozone [10], hydrogen peroxide [11], manganese dioxide [12], potassium permanganate [13], chlorine and chlorine dioxide [14]. However, to avoid the formation of dangerous oxidation by-

products and the presence of residuals in the treated water, photocatalysis can be a valid alternative [15–18]. Recently, several studies have been performed on the application of photocatalysis for the removal of arsenic from drinking water mainly using UV light active TiO_2 or other semiconductors, such as Fe_3O_4 [4]. For example, in our previous work, MoO_x/TiO_2 photocatalytst allowed to achieve total oxidation of As(III) to As(V) in water unlike of unmodified titania [19]. TiO_2 and zero-valent iron under simulated sunlight (Xe lamp) were also investigated and photocatalytic oxidation of As(III) to As(V) was found to be strongly affected by pH, being the optimal result observed at pH 3. [20] In order to make this process competitive with other consolidated options for full scale applications, photocatalysts synthesis process and operating costs (e.g., pH change, energy costs) should be cut down. To address this objective new visible light active photocatalysts easy to prepare (to reduce scale up costs) and that can successfully work under real conditions (e.g., neutral pH and real water matrix) are worthy of investigation. A novel bifunctional CuO-Fe_3O_4 material has been recently applied for As(III) removal through photooxidation and adsorption [4]. Interestingly, CuO-Fe_3O_4 nanoparticles can promote the photo-oxidation of As(III) to As(V) through CuO and As(V) adsorption through both CuO and Fe_3O_4. Although these photocatalytic

---

experiments were carried out in the presence of visible light (λ > 420 nm), a quite expensive (300 W Xe lamp) light source was used. Recently, the scientific community has developed a strong interest in another semiconductor: ZnO [21–30]. This photocatalyst has attracted an increasing attention due to its unique characteristics such as direct and wide band gap in the near-UV spectral region, strong oxidation ability, good photocatalytic property, and a large free-exciton binding energy [25,31]. Moreover, ZnO is relatively cheaper compared to TiO_2, which make it more attractive than TiO_2 for large scale water treatment applications [32]. In particular, as the removal of arsenic from drinking water is of concern, the use of ZnO for photocatalytic oxidation of As (III) to As (V) has been reported in the literature [33–38] and ZnO synthesis method affects its performance in the removal of contaminants from the water. Nidia Rivera-Reyna et al., observed the complete oxidation of As(III) by ZnO photocatalysis within 180 min of treatment at pH 8 [33]. In order to improve the photocatalytic performance of ZnO, as well as to make it active even under visible light irradiation to decrease treatment costs, different strategies were proposed in literature for ZnO doping. Among these, the introduction of different types of metal dopant into ZnO semiconductor, such as anionic dopant, cationic dopant and rare earth dopant, that could counter the recombination problem by enhancing the charge separation between electrons and holes, has been reported [39]. Anionic-doped ZnO photocatalyst enhanced the photocatalytic performances compared to that of pure ZnO. In the case of N doped ZnO system, the visible light absorption ability was found to increase [39,40]. Moreover, the structural, optical, chemical, electrical and magnetic properties of ZnO can be tuned by the addition of selected cationic dopant, such as Cu^{2+}, Ni^{2+}, Co^{2+} and Mn^{2+}. Cation-doped ZnO has a lower band gap energy value compared to the undoped ZnO. When cationic dopants were introduced as impurities in the ZnO crystal lattice, extra energy levels are added to the new photocatalyst [39]. In this regard, ZnO photocatalysts modified with copper have been proposed for the reactive black 5 degradation in presence of sunlight and in the acetaldehyde decomposition under visible light [41,42]. However, the literature concerning the use of ZnO doped with metals in photocatalytic oxidation of As(III) in As(V) under visible light as well as experiments under real conditions (namely neutral pH and real drinking water) is still scarce. Accordingly, the aim of this work was to investigate the photocatalytic performances of Cu-doped ZnO in the oxidation of As(III) in As(V) under real conditions in the effort to give a contribution to advance the knowledge and to make this process competitive with other consolidated technologies. In order to successfully address this objective, a simple method for the synthesis of Cu-doped ZnO was proposed, to obtain a visible light activate photocatalyst. Moreover, unlike of other works available in the scientific literature, a low energy consumption light source (LEDs) was investigated for the photocatalytic activation. The photocatalytic activity of the Cu-doped ZnO prepared at different Cu content and compared with the photocatalytic properties of undoped ZnO was assessed. The photocatalytic tests were carried out in aqueous matrices (deionized water solutions and real drinking water) using different As(III) initial concentrations and at the spontaneous pH of the solution.

2. Experimental

2.1. Photocatalyst preparation

2.1.1. Undoped ZnO catalyst

Undoped ZnO photocatalyst was prepared by the precipitation method starting from 5 g of zinc acetate dehydrate $ZnC_4H_6O_4$ (Aldrich, 99%) dissolved in 50 mL of distilled water and then by the slow addition of an aqueous solution obtained dissolving 2 g of NaOH (Aldrich, 99%) in 25 mL of distilled water at room temperature. Afterward, the generated precipitate was centrifuged, washed and calcined at 600°C for 2 h.

Table 1
Characterization results for the prepared photocatalysts.

Photocatalyst	Cu nominal amount [mol %]	Cu measured amount (XRF) [mol%]	*SSA [m²/g]	Band gap energy [eV]	**Crystallite size [nm]
ZnO	–	–	5.5	3.19	35
0.54Cu_ZnO	0.54	0.6	5.6	3.02	35
1.08Cu_ZnO	1.08	1.2	6.6	2.92	32
1.62Cu_ZnO	1.62	1.5	5.8	2.94	32
2.15Cu_ZnO	2.15	2.2	5.1	2.94	33
4.21Cu_ZnO	4.21	4.1	4.9	2.91	33

* B.E.T. method.
** Scherrer equation.

2.1.2. Cu-doped ZnO

Copper acetate hydrate $Cu(CH_3COO)$ was used in the doping procedure. Different amounts of $Cu(CH_3COO)$ were dissolved into the solution of $ZnC_4H_6O_4$ before to induce the precipitation by NaOH addition. The obtained precipitate was centrifuged, washed and calcined at 600 oC for 2 h. The Cu nominal loading is expressed as molar percentage and it was evaluated through Eq (1):

$$\%mol\ Cu = \frac{nCu}{nCu + nZn} \cdot 100 \tag{1}$$

Where:

nCu is the number of moles of $Cu(CH_3COO)_2$ used in the synthesis;
nZn is the number of moles of $Zn(CH_3COO)_2 \cdot 2H_2O$ used in the synthesis;

All the synthesized photocatalysts were listed in Table 1.

2.2. Photocatalysts characterization

The catalysts were characterized using different techniques. Specific surface area (SSA) of the samples was evaluated through Brunauer-Emmett-Teller (BET) method by N_2 adsorption with a Costech Sorptometer 1042 after a pretreatment at 150 °C for 1 h in He flow (99.9990%). Total Cu content of the samples was evaluated by X-ray fluorescence spectrometry (XRF) in a thermos Fischer ARL QUANT'X EDXRF spectrometer equipped with a rhodium standard tube as the source of radiation and with Si-Li drifted crystal detector. The Raman spectra of the samples were recorded with a Dispersive MicroRaman system (Invia, Renishaw), equipped with 514 nm diode-laser, in the range 100-2000 cm^{-1} Raman shift. The crystal phases of ZnO based photocatalysts were determined by XRD analysis carried out on Brucker D8 diffractometer, with a scan rate equal to 0.05 °/second (for the analysis in the range 20–80 degree), and 0.01 °/second (for the analysis in the range 30–34 degree). The crystallite size was calculated using the Scherrer equation. UV–vis reflectance spectra of the powder catalysts were recorded by a Perkin Elmer spectrometer Lambda 35 using a RSA-PE-20 reflectance spectroscopy accessory (Labsphere Inc., NorthSutton, NH). All spectra were obtained using an 8o sample positioning holder, giving total reflectance relative to a calibrated standard SRS-010-99 (Lab sphere Inc., North Sutton, NH). The reflectance data were elaborated in terms of Kubelka–Munk function [F(R∞)]. Band gap was calculated according to analytical methods available in the scientific literature and applied in a proper range selected to make the evaluation of absorption band edge reproducible and comparable [43]. In particular, band gap values were achieved by plotting $[F(R\infty) \times h\nu]^2$ vs $h\nu$ (eV) and by calculating the x intercept of a line passing through 0.5 < F (R∞) < 0.8. The morphology of the prepared samples was examined using a scanning electron microscope (Assing, mod. LEO 420).

2.3. Photocatalytic activity tests

A pyrex cylindrical batch reactor (ID = 2.5 cm; height = 18 cm)

equipped with an air distributor device (Q_{air} = 150 cm³/min under standard temperature and pressure conditions) and filled in with 100 mL of solution was used to test photocatalytic activity (photocatalyst dosage 3 g/L). The solution in the reactor was kept under continuous mixing conditions by a magnetic stirrer. Avisible-LEDs strip (nominal power: 10 W; light intensity: 32 mW/cm²) with wavelength emission in the range 400–600 nm (Figure S1) was used as light source. To make irradiation uniform and as much effective as possible, the LEDs strip was rolled up around the external surface of the reactor [44] which finally results in a distance between the light source and the solution varying from a minimum of 2 mm (corresponding to the internal surface of reactor thickness) to a maximum of 12.5 mm (corresponding to the reactor's radius). The reactor was left in dark condition for 2 h before to switch on visible LEDs. Photocatalytic reaction was carried out under light irradiation up to 3 h. In order to evaluate the photocatalytic activity of all prepared samples, preliminary tests with 10 mg/L methylene blue aqueous solutions containing were performed. In these conditions, the photocatalyst with the best performances in terms of dye degradation was selected. Subsequently, photocatalytic tests for the oxidation of As(III) in As(V) under visible light irradiation were performed. The effect of different initial As(III) concentrations (1.5, 2.5 and 5 mg/L) was also evaluated. Treated water samples were collected at fixed time to measure As(III) and As(V) concentration. In order to evaluate the radical scavengers effect and process performance in real water, photocatalytic tests were performed also with real drinking water purposely contaminated by As(III). In the latter case, in addition to the tests with visible LEDs, the efficiency of the optimized photocatalyst was also evaluated under simulated solar light by two 8 W Krypton-Argon lamps (SUN-GLO 8 W T5) whose emission spectrum is provided in Figure S2. The lamps were positioned at a distance of about 30 mm from the external surface of the photoreactor in order to irradiate the solution volume as much uniformly as possible.

2.4. Analytical measurements

Liquid samples were taken from the reactor at different times and analyzed with a Thermo Fisher Evolution 201 UV–Vis spectrophotometer to evaluate changes in dyes concentration through absorbance (λ = 663 nm) measurements. A spectrophotometric method based on the formation of molybdenum blue [19] was used for the analysis of As(V) concentration at λ = 880 nm. Total arsenic concentration in the solution was analyzed following a pre-oxidation step of As(III) through the addition of $KMnO_4$ aqueous solution (0.01 M). In this way residual As(III) was totally oxidized to As(V) before the measurement and then analyzed with the molybdenum blue method in both untreated and treated solutions [2]. Finally, As(III) and As(V) concentrations were calculated according to the following equations:

$$As_{tot} = As_{oxidized} - As_{reduced};$$

$$As(III) = As_{oxidized} - As_{untreated;}$$

$$As(V) = As_{untreated} - As_{reduced};$$

3. Results and discussion

3.1. Catalyst characterization

3.1.1. XRD analysis

XRD results of undoped and doped ZnO with different Cu content are reported in Fig. 1. The analysis in the range 20–80° (Fig. 1a) showed five main peaks at 31.90°, 34.58°, 36.43°, 47.08° and 56.72°, respectively indexed to the (1 0 0), (0 0 2), (1 0 1), (1 0 2) and (1 1 0) planes, typical of the hexagonal wurtzite crystal structure [45].

No trace of copper related phase (such as metallic copper or copper oxides) was detected for 0.54 mol % and 1.08 mol % Cu doped sample.

However, as doping percentage of Cu was increased up to 1.62 mol %, very weak peaks corresponding to CuO appeared [46], but they were found to grow in intensity as Cu doping was further increased (2.15 and 4.21 mol %).

Comparing the doped and undoped ZnO photocatalysts in the range 30–34° (Fig. 1b), a slight shift of XRD peaks towards higher angle was observed. This phenomenon is attributed to the narrowing of ZnO crystal lattice due to the substitution of Zn^{2+} by smaller Cu^{2+}, which suggests that Cu^{2+} can easily replace Zn^{2+} into ZnO crystal lattice [47,48], without modify the crystal structure of ZnO [46]. As matter of fact, due to ionic radius dimension of Cu^{2+} (0.73°A), which is very close to that of Zn^{2+} (0.74°A), Cu ions can easily penetrate into ZnO crystal lattice [46]. Moreover, the doping process induced a slight decrease of photocatalysts crystallite size (Table 1). The average crystallite size of the pure ZnO was 35 nm. As the Cu content was increased, the average crystalline size decreased to 32 nm. According to the literature, this slight decrease in the crystallites size could be due to foreign impurities of Cu^{2+} in the ZnO lattice, which decreases the nucleation and the subsequent ZnO growth rate [49].Accordingly, at smaller Cu doping concentrations, its ions can very well substitute Zn ions, but as Cu concentration increases, CuO starts to form cluster as impurity phase.

3.1.2. Raman analysis

Raman spectra in the range of 200-700 cm⁻¹ of doped catalysts and undoped ZnO are showed in Fig. 2.

In this range, there are four main bands at 333, 399, 438 and 583 cm⁻¹, related to ZnO [50]. The strong and sharp band observed at 438 cm⁻¹ corresponds to the non-polar optical phonons E_2 (high) mode of ZnO. The features located at 331 and 383 cm⁻¹ correspond to the multi-phonon scattering process E_2H–E_2L and A_1 (phonons of ZnO crystal, respectively) [51]. The signal located at 583 cm⁻¹ could be attributed to the E1, longitudinal optical phonon (LO) feature, associated with the formation of defects such as oxygen vacancy [52]. According to the literature, as the Cu doping concentration was increased, intensities of spectra decreased and the A1 transverse optical phonon (TO) mode vanished [53].

3.1.3. BET surface area and XRF results

The specific surface area (SSA) of all samples measured using BET gradually increased as Cu content was increased up to 1.08 mol % of Cu (Table 1).

However, a decrease of the SSA for samples with higher Cu doping (from 1.62 mol %), was observed. These results are in agreement with literature about Cu doped photocatalyst [54]. XRF results show that the real Cu content is consistent with the corresponding value of nominal metal content, supporting the conclusion that synthesis process was successful (Table 1).

3.1.4. SEM analysis

The surface morphology of the undoped ZnO and Cu doped ZnO photocatalyst has been analyzed by SEM and the obtained results are presented in Fig. 3.

In particular, for the sake of brevity, only the results for the ZnO samples, 1.08Cu_ZnO and 4.21Cu_ZnO were plotted. Both undoped and Cu-doped ZnO samples are composed of a number of non-uniform macro aggregates. Therefore the doping process did not affect the overall morphology of the photocatalysts.

3.1.5. UV–Vis diffuse reflectance spectra (UV–vis DRS)

Optical absorption properties of the catalysts were studied through UV–vis DRS in the range of 300–900 nm (Fig. 4).

Undoped ZnO showed the typical reflectance spectrum of UV active semiconducting materials with absorption onset at about 390 nm. This behavior is due to the electron transition from O 2p to Zn 3d, corresponding to the transition from the valence band to the conduction band, according to the energy band structure of ZnO [55]. The doping
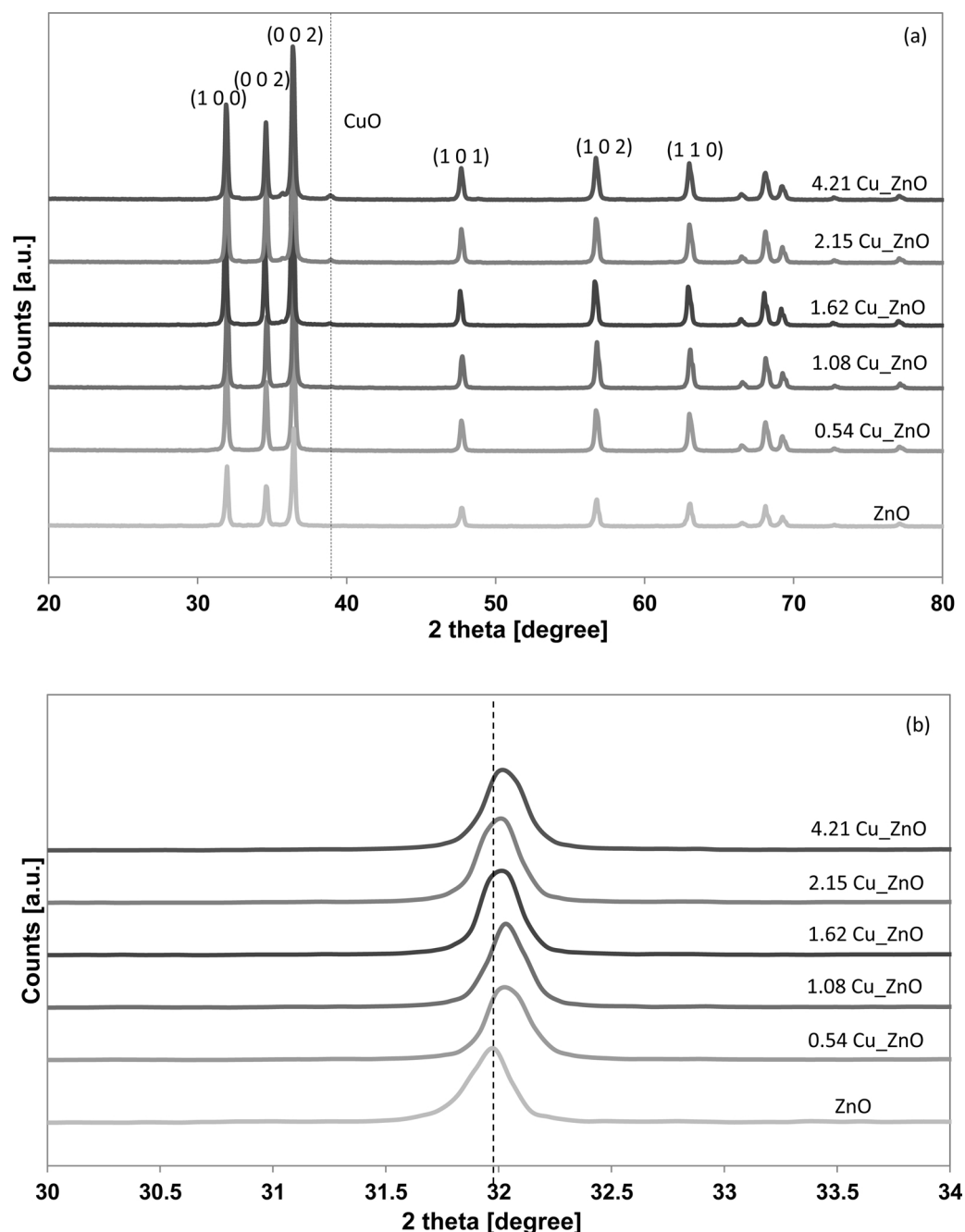
Fig. 1. XRD spectra of undoped ZnO and Cu-doped ZnO photocatalysts in the range 20–80° (a) and in the range 30–34° (b).

of ZnO with Cu leads to an improvement in the intensity of light absorption in the UV region, according to the literature [47]. It is worth noting that Cu doping resulted in an improvement of light absorption in the visible region, which could make the samples effective under solar light irradiation [56,57].

The data obtained from UV–vis reflectance spectra were used to evaluate the band-gap energy of the photocatalysts (Fig. 5 for undoped ZnO and 1.08Cu_ZnO and Figure S4 for the other prepared samples) summarized in Table 1.

As the Cu amount was increased, a decrease of band-gap energy (from 3.18 for undoped ZnO to 2.91 eV for 4.21Cu_ZnO) was measured. The observed decrease was due to the electronic transition from donor levels formed with dopants to the conduction band of the host photocatalysts [58].

3.2. Photocatalytic activity tests

3.2.1. Influence of Cu content

The photocatalytic activity of undoped ZnO and Cu-doped ZnO photocatalysts was evaluated trough the degradation of methylene blue (MB) (initial concentration 10 mg/L) under visible light (catalyst dosage: 3 g/L). As the dopant content was increased from 0.54 to 1.08 mol %, discoloration efficiency of MB increased, but further increases of dopant level resulted in a decreased MB degradation efficiency (Fig. 6a).

In particular, 1.08Cu_ZnO photocatalyst showed the highest photodegradation efficiency (52% of discoloration after 180 min of irradiation) compared to undoped ZnO and the other doped samples. According to the scientific literature, the improved photocatalytic performance is attributed to the synergic effect of Cu and ZnO, oxygen
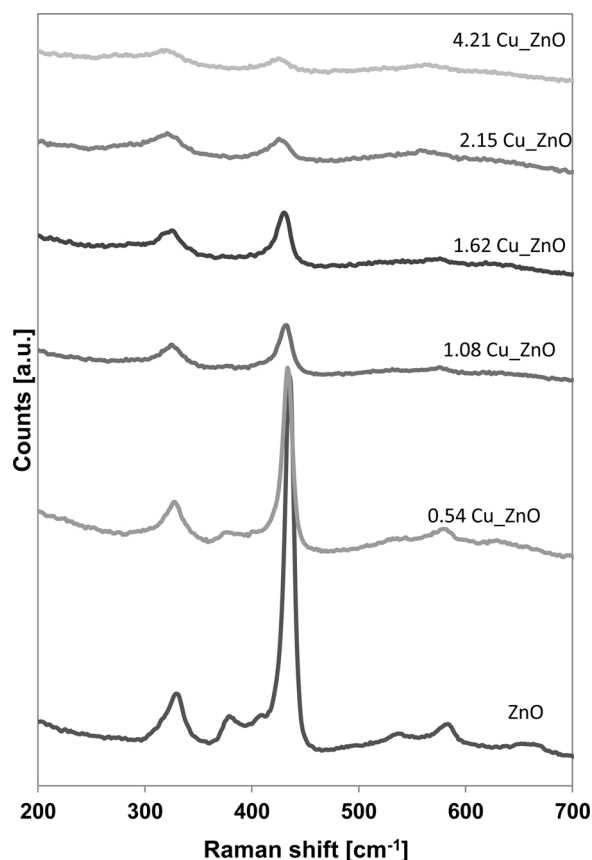
Fig. 2. Raman spectra of undoped ZnO and Cu-doped ZnO photocatalysts in the range 200-700 cm^{-1}.

Fig. 3. SEM images of undoped ZnO (a), 1.08Cu_ZnO (b) and 4.21Cu_ZnO (c) photocatalysts.

vacancy, decrease in size and suppressing the recombination rate of the electron-hole pairs [47]. However, the increase in Cu content beyond the optimal value led to a decrease in photocatalytic activity since the excess dopant content would acts as a recombination center of electron and hole pairs [59]. In order to analyze the recyclability of 1.08Cu_ZnO sample, the photocatalytic degradation of MB was repeated up to five cycles (Fig. 6b). The reduction of discoloration percentage was as low as 1–2% in 180 min of irradiation time. So, these results evidenced the stability of the photocatalyst and the possible absence of Cu leaching phenomena.

Once obtained the optimal content of doping in ZnO, the best photocatalyst (1.08Cu_ZnO) was used for the photocatalytic oxidation of As(III) to As(V).

3.2.2. Control tests on As(III) photocatalytic oxidation

In order to confirm the photocatalytic results obtained in the case of MB discoloration, control tests with only visible LEDs (photolysis test), undoped ZnO, 1.08Cu_ZnO and 2.15Cu_ZnO in presence of visible light, were carried out to evaluate the contribution of each process in the oxidation of As(III) (Fig. 7a) in As(V) (Fig. 7b) in liquid samples.

During photolysis test, both As(III) concentration decrease (initial concentration 5 mg/L) and As(V) increase were negligible. In presence of the tested photocatalysts, only the As(III) adsorption on the photocatalyst surface was observed during the dark phase, without As(V) formation. As LEDs were switched on, undoped ZnO was slightly effective for As(III) oxidation, whereas the two Cu-doped ZnO photocatalysts exhibited a very high photocatalytic activity in terms of oxidation of As(III) to As(V), even confirmed by the parallel increase of As(V) concentration in aqueous solution (Fig. 7b). In particular, at a fixed irradiation time, the photocatalytic performances of 1.08Cu_ZnO were better than those achieved for 2.15Cu_ZnO sample. The better oxidation
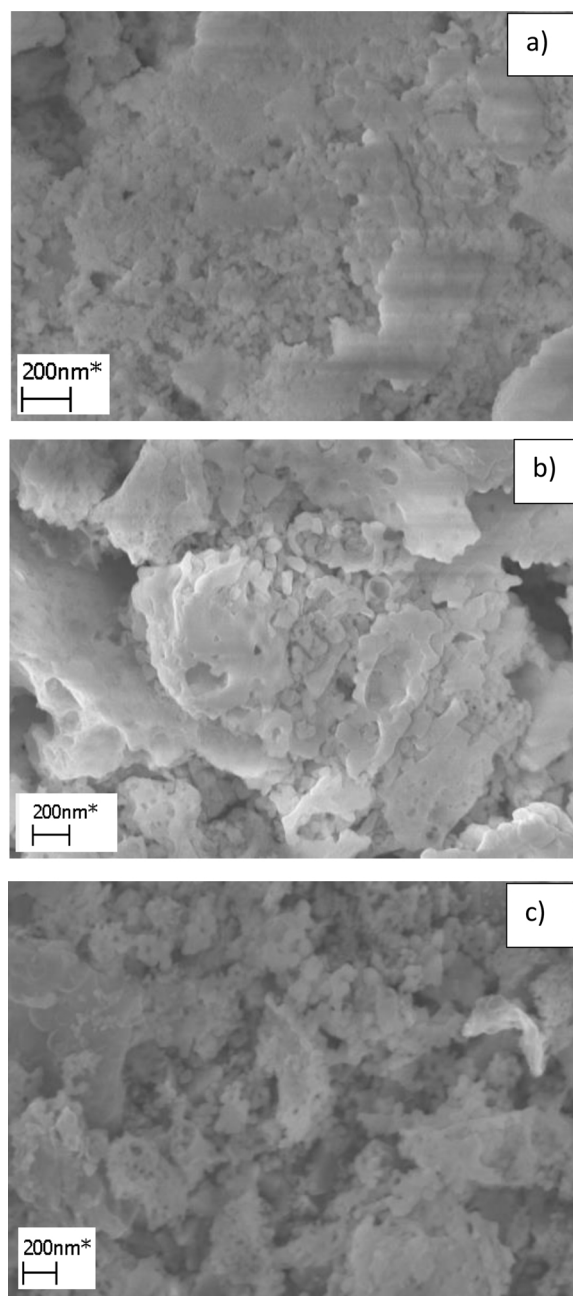
efficiency (almost complete removal of As(III) after 120 min of irradiation time) was achieved in the case of 1.08Cu_ZnO photocatalyst, confirming the results observed in the case of MB photodegradation tests (Fig. 6).

These results on the efficiency of Cu doped ZnO for the photocatalytic oxidation of As(III) are consistent with those documented in a previous work [33] and are extremely interesting as they show that the photocatalyst is effective even under visible light and at spontaneous pH (close to neutral values typical of drinking water). Although photocatalytic oxidation experiments of As(III) using ZnO have been reported in the literature, the best results in terms of As(III) oxidation (94% after 360 min of visible irradiation time) were obtained at pH equal to 8 [33]. The oxidation of As(III) in As(V) under visible light was investigated using Pt/TiO$_2$ nanotube electrode [60]. In this case, a bias was applied, and As(III) oxidation rate increased as a positive bias in the range 0.0–2.0 V was applied. In particular, As(III) in the cathodic
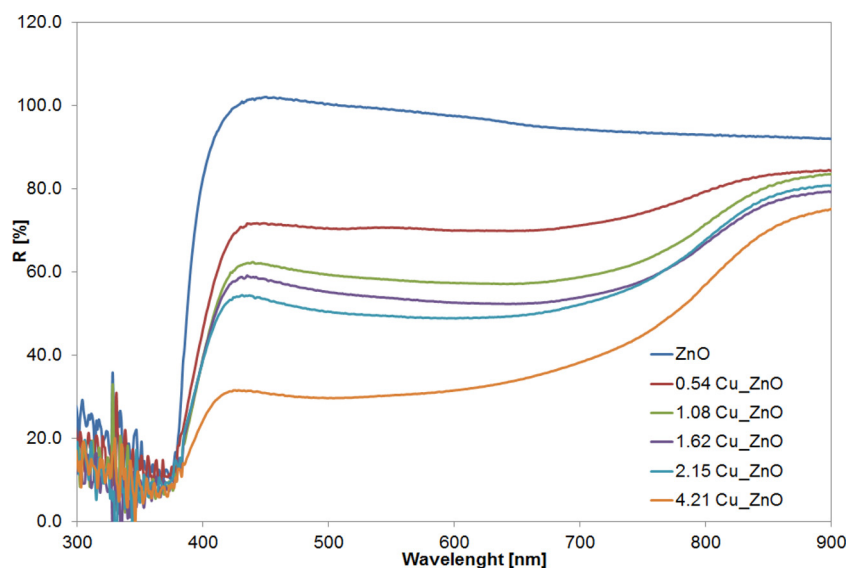
Fig. 4. UV–vis DRS spectra of ZnO and Cu-doped ZnO photocatalysts with different Cu contents. (For interpretation of the references to colour in this figure legend, the reader is referred to the web version of this article).
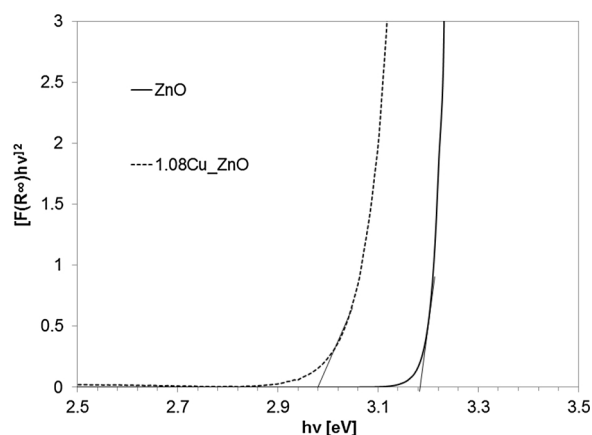

Fig. 5. Evaluation of band gap for undoped ZnO and 1.08Cu_ZnO photocatalyst.

cell was completely oxidized into As(V) after 280 min of irradiation time and 2.0 V of positive bias potential [60].

3.2.3. Optimization of catalyst dosage for photocatalytic tests

Different amounts of 1.08Cu_ZnO (in the range 0.75–4.5 g/L) were investigated to optimize photocatalysts dose (Fig. 8).

As the amount of catalyst in the solution was increased, an almost linear increase of photocatalytic efficiency up to a dosage of 3 g/L was observed (70% of As(V) yield obtained after 180 min of visible light irradiation). According to a previous work, the photocatalytic reaction mechanism on the ZnO based photocatalyst is expected to mainly proceed by HO· radicals and to a lesser extent by the contribution of holes [33,61]. Therefore, it is possible to argue that the increase in the catalyst dose up to 3 g/L provides more active sites on the 1.08Cu_ZnO surface, resulting in an increased amount of hydroxyl radicals. Beyond 3 g/L catalyst dosage, the photocatalytic performances decreased (37% of As(V) yield with a dosage equal to 4.5 g/L against 70% As(V) yield achieved with 3 g/L catalyst loading). The worsening of photocatalytic activity as photocatalyst dose was increased may be explained by the increased opacity of the aqueous solution which made light penetration through the solution increasingly difficult [19]. Therefore 3 g/L of photocatalyst loading was considered as the optimum dose and it was used to evaluate the influence of initial As(III) concentration in aqueous solution and the effect of a real water matrix.
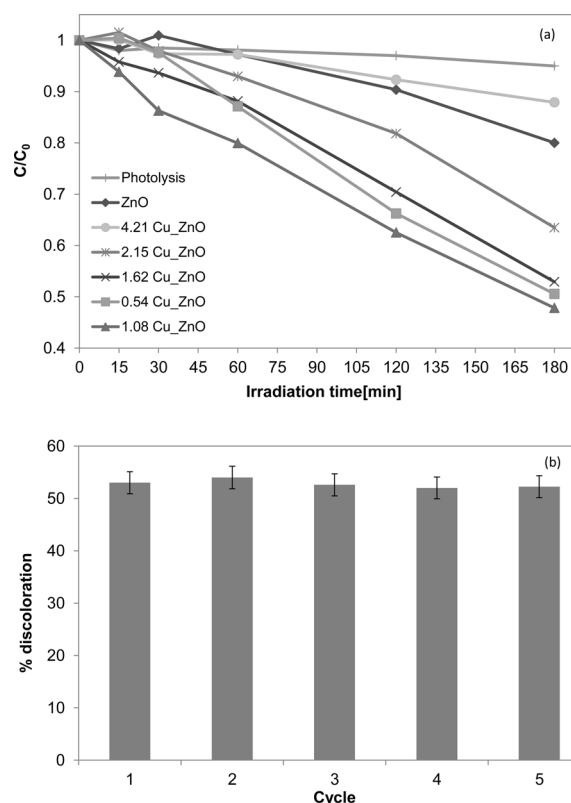

Fig. 6. Behavior of methylene blue relative concentration during the irradiation time for all the photocatalysts (a) and evaluation of methylene blue discoloration after 180 min of visible irradiation on 1.08Cu_ZnO catalyst for different cycles (b); methylene blue initial concentration: 10 mg/L; catalyst dosage: 3 g/L (For interpretation of the references to colour in this figure legend, the reader is referred to the web version of this article).
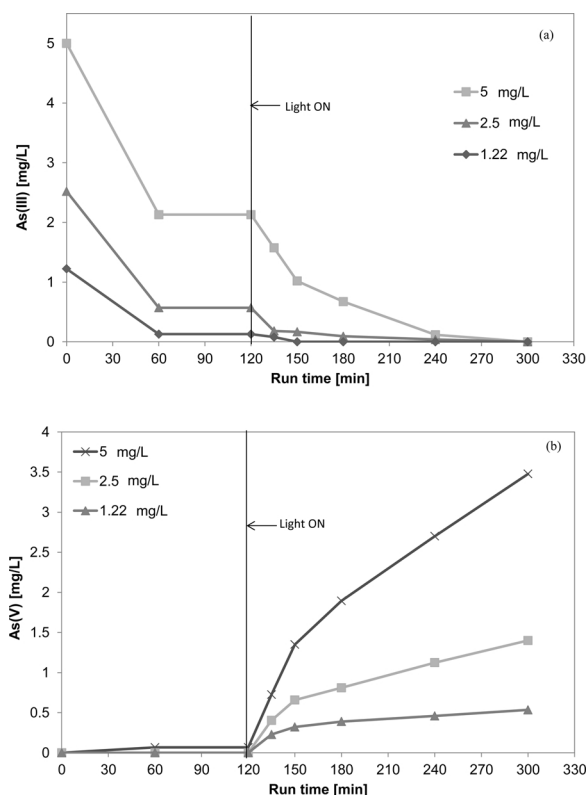
3.2.4. Effect of the initial concentration of As (III) on the photocatalytic process

The effect of the initial concentration of As(III) on the photocatalytic oxidation of As(III) to As(V) using 1.08Cu_ZnO catalyst was investigated too (Fig. 9).
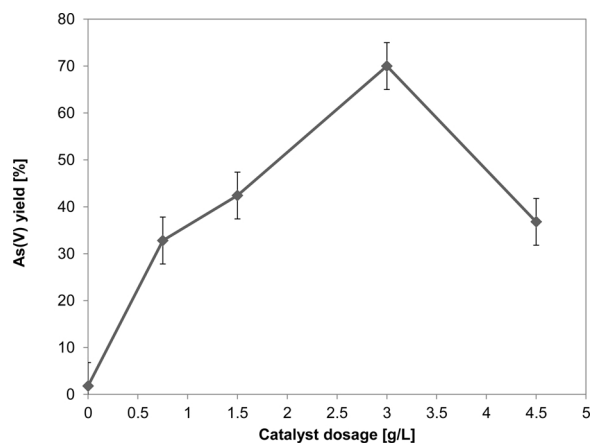
The residual concentration of As(III) decreased during both dark
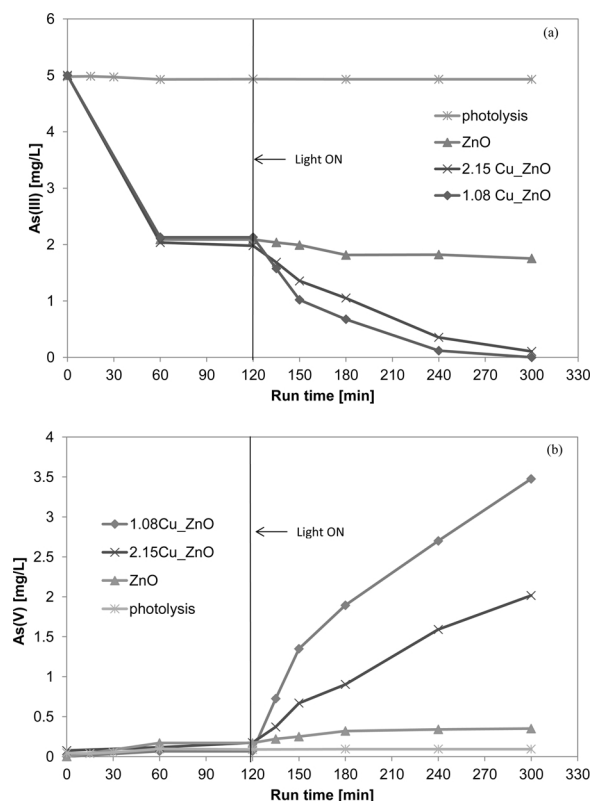
Fig. 7. Control tests for the photocatalytic oxidation of As(III). Initial As(III) concentration: 5 mg/L. Catalyst dosage: 3 g/L. Behavior of As (III) (a) and As(V) (b) concentration.

Fig. 8. As(V) yield after 3 h of irradiation time as a function of catalyst dosage. Initial As(III) concentration: 5 mg/L; photocatalyst: 1.08 Cu_ZnO.

and visible light phases for the three initial As(III) concentrations investigated (1.22, 2.5 and 5 mg/L). However, the process was strongly affected by the amount of As(III) adsorbed in dark conditions, in agreement with a previous study [33]. As matter of fact, the irradiation time necessary to achieve the complete As(III) removal increased with the increase of the initial As(III) concentration in solution and in particular, at lowest tested initial As(III) concentration (1.22 mg/L), the optimized 1.08Cu_ZnO photocatalyst is able to ensure the complete removal of As(III) after only 30 min of visible light irradiation.

3.2.5. Photocatalytic tests in drinking water

In order to evaluate the effectiveness of the photocatalysts in a real water matrix, photocatalytic tests with real drinking water (chemical-


Fig. 9. Effect of the initial concentration of As(III) on photocatalytic performances. Behavior of As(III) (a) and As(V) (b); photocatalyst: 1.08 Cu_ZnO; photocatalyst dosage: 3 g/L.

Table 2
Physical and chemical characteristics of drinking water.

pH	7.2
Conductivity, $\mu S/$ cm	181
Total hardness,°F	4.00
Sodium, mg /l	7.05
Potassium, mg /l	7.30
Calcium, mg /l	18.27
Magnesium, mg /l	5.99
Chlorides (Cl^-),mg /l	8.20
Sulfates (SO_4^{2-}),mg /l	2.90
Bicarbonates (HCO_3^-),mg /l	103.7
Nitrates (NO_3^-),mg /l	2.00

physical characteristics in Table 2) were also carried out (Fig. 10).

It is well known that ionic species like bicarbonates and chlorides act as radical scavengers in photocatalytic processes [62,63], so it is interesting to understand if their presence, even at low concentrations as in this case, affect process efficiency. In particular, the comparison in terms of As(III) oxidized and As(V) present in solution in the case of (i) distilled water under visible LEDs, (ii) drinking water under visible LEDs and (iii) drinking water under solar lamp, is shown (Fig. 10). The difference between the two matrices (distilled and drinking water) is evident during the dark adsorption phase, where a higher adsorption of As(III) on the catalyst surface in the case of the distilled water matrix was observed with respect to the As(III) adsorption in drinking water. However, in the presence of visible light, the efficiency of the photocatalyst is maintained also in drinking water. It is worthy to note that, in the latter case, after 180 min of both visible light irradiation and simulated solar light, the As(V) concentration is almost equal to the As (III) initial concentration. This result shows that the 1.08Cu_ZnO photocatalyst is able to completely oxidize As (III) into As (V) which is released in the solution without occupying the active sites, similarly to
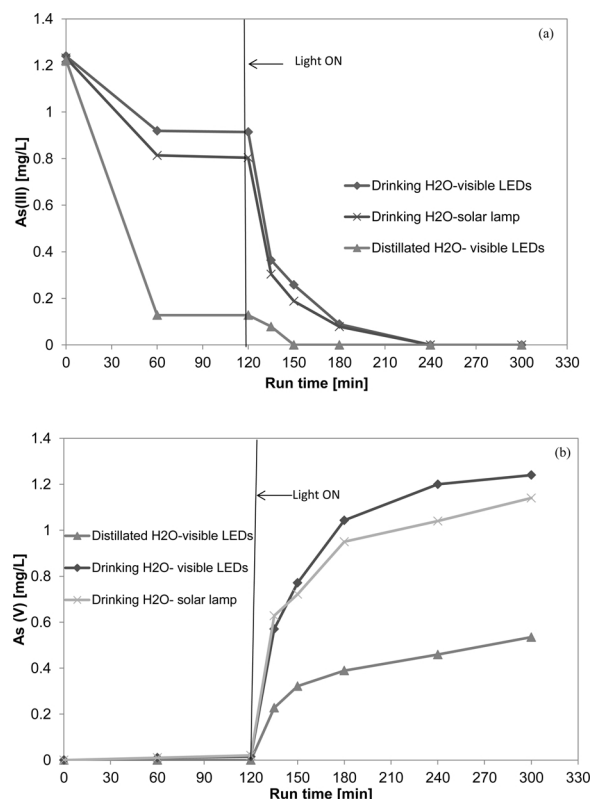
Fig. 10. Photocatalytic oxidation of As(III) in distillated and drinking water. Behavior of As(III) (a) and As(V) (b) concentration. Initial As(III) concentration: 1.22 mg/L; photocatalyst: 1.08 Cu_ZnO; photocatalyst dosage: 3 g/L.

what observed in previous works using MoO_x/TiO_2 photocatalyst in the arsenite oxidation to arsenate under UV light [2,19,62].

4. Conclusions

The possibility to obtain an efficient oxidation of As (III) in As (V) has been demonstrated in this work by applying a photocatalytic process based on the use of Cu-doped ZnO photocatalysts active under visible light and real conditions (neutral pH and real drinking water). The characterization of the photocatalysts showed that the crystal structure of all samples is hexagonal wurtzite with an average crystallite sizes approximately in the range 32–33 nm. Moreover the doping with Cu allowed to obtain a decrease of band gap energy from 3.2 eV, typical of pure ZnO, up to 2.92 eV. The best photocatalytic performances were obtained with 1.08 mol% of Cu (1.08Cu_ZnO). In particular, a complete oxidation of As(III) (at 5 mg/L initial concentration) to As(V) was achieved within 120 min under visible LEDs. Moreover the experimental results highlighted the efficiency of this photocatalyst even with different initial concentrations of As (III) in solution. In particular, the total oxidation of As(III) was obtained after only 30 min of irradiation starting from an initial concentration of As(III) equal to 1.22 mg/L. It is worthy to mention that these results were obtained under the spontaneous pH of the solution (almost neutral pH), typical of drinking water. Finally, excellent performances even in the presence of solar simulated light and real drinking water were observed. In particular, As(V) concentration was found to be almost equal to the As(III) initial concentration after 180 min under both visible light and simulated solar light, evidencing that the 1.08Cu_ZnO photocatalyst is able to completely oxidize As (III) to As (V) which is released in the solution (and consequently it can be removed by a conventional adsorption process) without saturating photocatalyst active sites. This result will make photocatalyst life longer, which together with high process efficiency under neutral conditions, makes this process more attractive

compared to other photocatalytic processes investigated so far.

Appendix A. Supplementary data

Supplementary material related to this article can be found, in the online version, at doi:https://doi.org/10.1016/j.apcatb.2018.07.026.

References

[1] C.K. Jain, I. Ali, Water Res. 34 (2000) 4304–4312.
[2] V. Vaiano, G. Iervolino, D. Sannino, L. Rizzo, G. Sarno, Chem. Eng. Res. Des. 109 (2016) 190–199.
[3] R.R. Shrestha, M.P. Shrestha, N.P. Upadhyay, R. Pradhan, R. Khadka, A. Maskey, M. Maharjan, S. Tuladhar, B.M. Dahal, K. Shrestha, J. Environ. Sci. Health - Part A Toxic/Hazard. Substances and Environ. Eng. 38 (2003) 185–200.
[4] T. Sun, Z. Zhao, Z. Liang, J. Liu, W. Shi, F. Cui, J. Colloid Interface Sci. 495 (2017) 168–177.
[5] R.M. Dhoble, S. Lunge, A.G. Bhole, S. Rayalu, Water Res. 45 (2011) 4769–4781.
[6] V.K. Sharma, M. Sohn, Environ. Int. 35 (2009) 743–759.
[7] P. Bahmani, A. Maleki, H. Daraei, M. Khamforoush, R. Rezaee, F. Gharibi, A.G. Tkachev, A.E. Burakov, S. Agarwal, V.K. Gupta, J. Colloid Interface Sci. 506 (2017) 564–571.
[8] M. Bhaumik, C. Noubactep, V.K. Gupta, R.I. McCrindle, A. Maity, Chem. Eng. J. 271 (2015) 135–146.
[9] M. Bissen, F.H. Frimmel, Acta Hydrochim. Hydrobiol. 31 (2003) 97–107.
[10] M.-J. Kim, J. Nriagu, Sci. Total Environ. 247 (2000) 71–79.
[11] M. Pettine, L. Campanella, F.J. Millero, Geochim. Cosmochim. Acta 63 (1999) 2727–2735.
[12] W. Driehaus, R. Seith, M. Jekel, Water Res. 29 (1995) 297–305.
[13] A. Hussam, A.K.M. Munir, J. Environ. Sci. Health 42 (Part A) (2007) 1869–1878.
[14] S. Sorlini, F. Gialdini, Water Res. 44 (2010) 5653–5659.
[15] A. Nikolaou, L. Rizzo, H. Selcuk, Control of Disinfection by-Products in Drinking Water Systems, (2007).
[16] S. Zhang, J. Li, X. Wang, Y. Huang, M. Zeng, J. Xu, ACS Appl. Mater. Interfaces 6 (2014) 22116–22125.
[17] S. Zhang, J. Li, X. Wang, Y. Huang, M. Zeng, J. Xu, J. Mater. Chem. A 3 (2015) 10119–10126.
[18] D. Zhao, G. Sheng, C. Chen, X. Wang, Appl. Catal. B 111-112 (2012) 303–308.
[19] V. Vaiano, G. Iervolino, D. Sannino, L. Rizzo, G. Sarno, A. Farina, Appl. Catal. B 160-161 (2014) 247–253.
[20] M.J. López-Muñoz, A. Arencibia, Y. Segura, J.M. Raez, Catal. Today 280 (2017) 149–154.
[21] P. Goyal, S. Chakraborty, S.K. Misra, Environ. Nanotechnol. Monit. Manag. 10 (2018) 28–35.
[22] S. Duo, R. Zhong, Z. Liu, J. Wang, T. Liu, C. Huang, H. Wu, J. Phys. Chem. Solids 120 (2018) 20–33.
[23] P. Pascariu, I.V. Tudose, M. Suchea, E. Koudoumas, N. Fifere, A. Airinei, Appl. Surf. Sci. 448 (2018) 481–488.
[24] T. Iqbal, M.A. Khan, H. Mahmood, Mater. Lett. 224 (2018) 59–63.
[25] V. Vaiano, G. Iervolino, J. Colloid Interface Sci. 518 (2018) 192–199.
[26] V. Vaiano, M. Matarangolo, J.J. Murcia, H. Rojas, J.A. Navío, M.C. Hidalgo, Appl. Catal. B 225 (2018) 197–206.
[27] C. Jaramillo-Páez, J.A. Navío, M.C. Hidalgo, J. Photochem. Photobiol. A Chem. 356 (2018) 112–122.
[28] R. Saravanan, S. Agarwal, V.K. Gupta, M.M. Khan, F. Gracia, E. Mosquera, V. Narayanan, A. Stephen, J. Photochem. Photobiol. A Chem. 353 (2018) 499–506.
[29] L. Gnanasekaran, R. Hemamalini, R. Saravanan, K. Ravichandran, F. Gracia, S. Agarwal, V.K. Gupta, J. Photochem. Photobiol. B, Biol. 173 (2017) 43–49.
[30] M.H. Dehghani, P. Mahdavi, I. Tyagi, S. Agarwal, V.K. Gupta, Desalination Water Treat. 57 (2016) 24359–24367.
[31] A. Janotti, C.G. Van de Walle, Rep. Prog. Phys. 72 (2009) 126501/126501-126501/126529.
[32] N. Daneshvar, D. Salari, A.R. Khataee, J. Photochem. Photobiol. A Chem. 162 (2004) 317–322.
[33] N. Rivera-Reyna, L. Hinojosa-Reyes, J.L. Guzman-Mar, Y. Cai, K. O'Shea, A. Hernandez-Ramirez, Photochem. Photobiol. Sci. 12 (2013) 653–659.
[34] M. Arabnezhad, M. Shafiee Afarani, A. Jafari, Int. J. Environ. Sci. Technol. (2017).
[35] K. Khwamsawat, J. Mahujchariyawong, S. Danwittayakul, Using ZnO nanorods coated porous ceramic monolith to remove arsenic from groundwater, Key Eng. Mater. (2017) 756–765.
[36] A.A. Alswata, M.B. Ahmad, N.M. Al-Hada, H.M. Kamari, M.Z.B. Hussein, N.A. Ibrahim, Results Phys. 7 (2017) 723–731.
[37] C. Miranda, P. Santander, J. Matschullat, B. Daus, J. Yáñez, H.D. Mansilla, J. Adv. Oxid. Technol. 19 (2016) 276–283.
[38] A. Samad, M. Furukawa, H. Katsumata, T. Suzuki, S. Kaneco, J. Photochem. Photobiol. A Chem. 325 (2016) 97–103.
[39] K.M. Lee, C.W. Lai, K.S. Ngai, J.C. Juan, Water Res. 88 (2016) 428–448.
[40] M. Batzill, E.H. Morales, U. Diebold, Phys. Rev. Lett. 96 (2006) 026103/026101-026103/026104.
[41] T. Arai, S.-i. Senda, Y. Sato, H. Takahashi, K. Shinoda, B. Jeyadevan, K. Tohji, Chem. Mater. 20 (2008) 1997–2000.
[42] S. Anandan, M. Miyauchi, J. Chem. Soc. Faraday Trans. 13 (2011) 14937–14945.
[43] C. Anderson, A.J. Bard, J. Phys. Chem. B 101 (1997) 2611–2616.

[44] G. Iervolino, V. Vaiano, D. Sannino, L. Rizzo, V. Palma, Appl. Catal. B 207 (2017) 182–194.

[45] O. Yayapao, T. Thongtem, A. Phuruangrat, S. Thongtem, Mater. Sci. Semicond. Process. 39 (2015) 786–792.

[46] S. Singhal, J. Kaur, T. Namgyal, R. Sharma, Phys. B Condens. Matter 407 (2012) 1223–1226.

[47] A.N. Kadam, T.G. Kim, D.S. Shin, K.M. Garadkar, J. Park, J. Alloys 710 (2017) 102–113.

[48] S.P. Meshram, P.V. Adhyapak, D.P. Amalnerkar, I.S. Mulla, Ceram. Int. 42 (2016) 7482–7489.

[49] P.K. Sharma, M. Kumar, A.C. Pandey, J. Nanoparticle Res. 13 (2011) 1629–1637.

[50] Q. Zhang, J.-K. Liu, J.-D. Wang, H.-X. Luo, Y. Lu, X.-H. Yang, Ind. Eng. Chem. Res. 53 (2014) 13236–13246.

[51] Q.-P. Luo, X.-Y. Yu, B.-X. Lei, H.-Y. Chen, D.-B. Kuang, C.-Y. Su, J. Phys. Chem. C 116 (2012) 8111–8117.

[52] V. Vaiano, M. Matarangolo, O. Sacco, D. Sannino, Appl. Catal. B 209 (2017) 621–630.

[53] P. Ilanchezhiyan, G.M. Kumar, M. Subramanian, R. Jayavel, Mater. Sci. Eng. B 175 (2010) 238–242.

[54] P. Pongwan, K. Wetchakun, S. Phanichphant, N. Wetchakun, Res. Chem. Intermed. 42 (2016) 2815–2830.

[55] L. Zhang, Y. Yang, R. Fan, J. Yu, L. Li, J. Mater. Chem. A 1 (2013) 12066–12073.

[56] S. Kuriakose, B. Satpati, S. Mohapatra, J. Chem. Soc. Faraday Trans. 17 (2015) 25172–25181.

[57] P. Bandyopadhyay, A. Dey, R. Basu, S. Das, P. Nandy, Curr. Appl. Phys. 14 (2014) 1149–1155.

[58] W. Wang, M.O. Tadé, Z. Shao, Chem. Soc. Rev. 44 (2015) 5371–5408.

[59] P. Chen, J. Mater. Sci. Mater. Electron. 27 (2016) 2394–2403.

[60] Y. Qin, Y. Li, Z. Tian, Y. Wu, Y. Cui, Nanoscale Res. Lett. 11 (2016) 32.

[61] M.E. Pena, G.P. Korfiatis, M. Patel, L. Lippincott, X. Meng, Water Res. 39 (2005) 2327–2337.

[62] G. Iervolino, V. Vaiano, L. Rizzo, G. Sarno, A. Farina, D. Sannino, J. Chem. Technol. Biotechnol. 91 (2016) 88–95.

[63] A. Ziylan-Yavaş, N.H. Ince, Chemosphere 162 (2016) 324–332.